LASER & PHOTONICS REVIEWS
www.lpr-journal.org

A White-Box Digital Twin for Real-Time Polarization Tracking

Xuguang Zhang, Guoqing Pu, Yong Wu, Weisheng Hu, and Lilin Yi**

Tracking polarization in real-time is a long-term challenge. The conventional heuristic and gradient-descent-based algorithms for polarization tracking lack efficiency and interpretability. To resolve the problem, a white-box digital twin modeling the entire polarization tracking system is derived by calculating with Stokes vectors and Mueller matrices. Moreover, the real-time polarization tracking enabled by the white-box digital twin is experimentally demonstrated, which is over 7 times faster than the commonly used stochastic parallel gradient descent (SPGD) on average. The adoption of digital twin allows the algorithm to bypass the loop of perturbation, sampling, and adjusting over the real system, thereby significantly reducing the sample times and recovery time. The proposed white-box digital-twin-based algorithm has strong interpretability and high efficiency, which has substantial potential to become a standard approach to achieve real-time polarization tracking.

1. Introduction

A stable state of polarization (SOP) is always desired in diverse optical applications ranging from quantum communication,[1–5] quantum computation,[6–9] gravitational-wave observatory,[10–12] and coherent beam combining[13–16] to coherent optical communication.[17–19] However, due to defects of fiber, mechanical and thermal disturbances, air turbulence, etc.,[20–25] the SOP of light varying stochastically in transmission calls for real-time polarization tracking techniques, which is a long-term challenge. The conventional algorithms for SOP tracking generally include various heuristic algorithms and gradient-descent-based algorithms. Heuristic algorithms, such as genetic algorithm (GA),[26] simulated annealing (SA),[27] particle swarm optimization (PSO),[28] etc., are computationally intensive thereby demanding hundreds of interactions with the real system to complete SOP tracking and their performances heavily depend on the hyper-parameters tuning. As the alternative, gradient-descent-based algorithms become more popular, such as the most popular stochastic parallel gradient descent (SPGD),[29,30] root mean square propagation (RMSprop),[31] adaptive moment estimation (Adam),[32] etc. Their performances also depend on hyper-parameters tuning and related techniques to avoid zigzag, for instance, the adaptive learning rate strategy and momentum. Particularly, various random noises in the real system inevitably introduce errors in gradient calculations, which could be fatal to these gradient-descent-based algorithms. Moreover, both heuristic and gradient-descent-based algorithms are generally blind-searching algorithms lacking interpretability and efficiency. There is barely theoretical assurance that any algorithm can eventually compensate for the SOP disturbances. On the other hand, the indeterminacy of blind-searching demands more necessary sample times, further increasing the time consumption of achieving the target SOP. Among all existing algorithms, the SPGD generally requires the least sample times (i.e., usually dozens of sample times), thereby making it the most popular solution to polarization tracking.

Here, we demonstrate real-time polarization tracking enabled by a white-box digital twin modeling the entire polarization tracking system. Via modeling with Stokes vectors and Mueller matrices, we derive that the output optical power can be expressed by a linear assembly of 9 simple terms with 9 coefficients waiting to be resolved. As a result, merely 9 sample times are required to establish the digital twin. Then, the optimal control state can be searched in the digital twin, and one-step polarization tracking is achieved. The introduction of the white-box digital twin enables us to save numerous sample times from the real system. We conduct experiments to test the recovery time of achieving target SOP after disturbance and the optical power under various disturbances and to compare performances of the digital-twin-based algorithm with the commonly used SPGD in polarization tracking. The experimental results show that the digital-twin-based real-time polarization tracking is on average over 7 times faster than the SPGD in an identical physical setup. On the other hand, the SPGD is rather sensitive to the initial state due to the lack of global information on the objective function. The problem is perfectly resolved by the white-box digital twin providing the accurate global landscape of the objective function. Consequently, the digital-twin-based algorithm is way more robust than the SPGD in diverse polarization disturbances. Further, via combining the white-box digital twin with the SPGD, more powerful and robust real-time continuous polarization tracking is experimentally demonstrated. The introduction of the white-box digital twin greatly improves the stability, determinacy, and interpretability of polarization tracking.

X. Zhang, G. Pu, Y. Wu, W. Hu, L. Yi
State Key Lab of Advanced Communication Systems and Networks
School of Electronic Information and Electrical Engineering
Shanghai Jiao Tong University
Shanghai 200240, China
E-mail: teddyghf1994@sjtu.edu.cn; lilinyi@sjtu.edu.cn

The ORCID identification number(s) for the author(s) of this article can be found under https://doi.org/10.1002/lpor.202400076

DOI: 10.1002/lpor.202400076

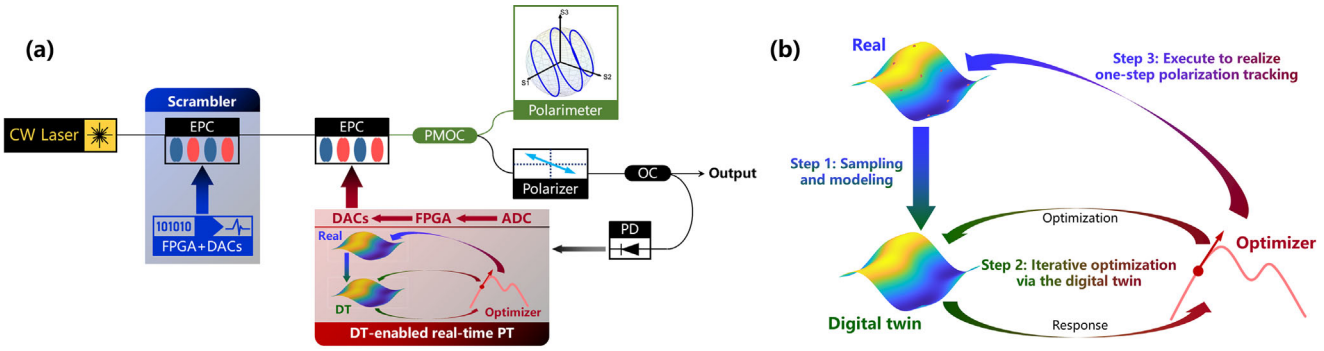

Figure 1. a) The experimental setup of polarization tracking. The continuous wave (CW) laser and the homemade scrambler together generate a light beam with random SOP, which passes through an electrical polarization controller (EPC) for polarization tracking. The polarization maintaining optical coupler (PMOC) splits the light beam into two. One beam is sent to a polarimeter to measure the SOP. The other transmits through the polarizer and part of it is used for feedback after being acquired by an analog-to-digital converter (ADC). The real-time polarization tracking (PT) is completed by the field programmable gate array (FPGA) controlling digital-to-analog converters (DACs) after running the digital-twin(DT)-based algorithm. b)The workflow of the digital-twin-based polarization tracking algorithm. First, establish the digital twin with 9 fixed samples from the real system. Then, the optimizer searches the set of phase retardances corresponding to the maximum output power via the digital twin. Finally, apply the searched phase retardances to the real system.

2. Principles

2.1. Experimental Setup

The experimental setup is shown in **Figure** 1a. In this polarization tracking system, the light beam is generated by a continuous wave (CW) linear-polarized laser centering at 1550 nm and first transmits through a homemade polarization scrambler. The homemade polarization scrambler is composed of an EPC and its corresponding control circuits which include a field programmable gate array (FPGA) and the affiliated digital-to-analog converters (DACs) to control the electrical polarization controller (EPC). The polarization scrambler can effectively randomly disturb the SOP. The light beam with random SOP passes through the other EPC to compensate for the polarization disturbances introduced by the scrambler. The EPCs in this system consist of four phase retarders whose phase retardance is proportional to the square of the corresponding analog DC driving voltage. The typical half-wave voltage of the phase retarder is 123 V. The azimuths of four retarders are sequentially 0, 45, -45, and 0°. Note that similar effects can be achieved with other types of EPCs, for instance, the EPCs consisting of retarders with fixed azimuths and variable retardances, and the EPCs based on squeezing fiber with PZT. The light beam after compensation is split into two beams by a polarization maintaining optical coupler (PMOC). One beam is sent to a polarimeter to measure the SOP, and the other transmits through a polarizer, which transfers the SOP variations into fluctuations of optical power. A photodetector (PD) and an optical coupler (OC) are employed to detect the power of the transmitted light beam at a fixed ratio and to generate a feedback analog voltage signal for the analog-to-digital converter (ADC) to sample. Finally, the polarization tracking is completed by the FPGA controlling DACs after calculations in situ. When the output power of the polarizer reaches the maximum, the input SOP of the polarizer aligns with the orientation of the polarizer, thereby achieving polarization tracking. Note the polarization maintaining links highlighted in green in Figure 1a are merely utilized to measure the SOP, which is unnecessary in actual polarization tracking systems.

2.2. Theory of the White-Box Digital Twin

Consider a typical system containing two variable phase retarders and a polarizer. We calculate SOPs using Stokes vectors and Mueller matrices. The Mueller matrix of a variable phase retarder is

$$M(\theta,\Delta) = \begin{bmatrix} 1 & 0 & 0 & 0 \\ 0 & \cos^2 2\theta + \sin^2 2\theta \cdot \cos\Delta & \sin 2\theta \cdot \cos 2\theta \cdot (1-\cos\Delta) & -\sin 2\theta \cdot \sin\Delta \\ 0 & \sin 2\theta \cdot \cos 2\theta \cdot (1-\cos\Delta) & \sin^2 2\theta + \cos^2 2\theta \cdot \cos\Delta & \cos 2\theta \cdot \sin\Delta \\ 0 & \sin 2\theta \cdot \sin\Delta & -\cos 2\theta \cdot \sin\Delta & \cos\Delta \end{bmatrix} \tag{1}$$

where θ and Δ are respectively the azimuth and the retardance of the retarder.[33] The Mueller matrix of a polarizer is

$$M(\theta) = \frac{1}{2}\begin{bmatrix} 1 & \cos 2\theta & \sin 2\theta & 0 \\ \cos 2\theta & \cos^2 2\theta & \sin 2\theta \cdot \cos 2\theta & 0 \\ \sin 2\theta & \sin 2\theta \cdot \cos 2\theta & \sin^2 2\theta & 0 \\ 0 & 0 & 0 & 1 \end{bmatrix} \tag{2}$$

where θ is the azimuth of the polarizer.[33] The Stokes vector of the output light beam $\boldsymbol{S}'$ is

$$\boldsymbol{S}' = \begin{bmatrix} S_0' & S_1' & S_2' & S_3' \end{bmatrix}^T = M_N \cdots M_2 M_1 \boldsymbol{S} \tag{3}$$

where $\boldsymbol{S}$ is the Stokes vector of the input light beam, and $M_1, M_2, \ldots, M_N$ are the Mueller matrices of optical components

as the sequence that the light beam passes through.[33] The first element of Stokes vector $\boldsymbol{S}'$ is S_0', which indicates the power of the output light beam. In this system, the azimuths of all optical components are fixed. So, all terms in Mueller matrices of optical components, except the terms containing the phase retardances of the two phase retarders, are also fixed. We can derive that the optical output power γ can be expressed as

$$\gamma = S_0' = \begin{bmatrix}1\\0\\0\\0\end{bmatrix}^T \boldsymbol{S}' = \begin{bmatrix}a_1\\a_2\\a_3\\a_4\\a_5\\a_6\\a_7\\a_8\\a_9\end{bmatrix}^T \cdot \begin{bmatrix}1\\\sin\Delta_1\\\cos\Delta_1\\\sin\Delta_2\\\cos\Delta_2\\\sin\Delta_1\cdot\sin\Delta_2\\\sin\Delta_1\cdot\cos\Delta_2\\\cos\Delta_1\cdot\sin\Delta_2\\\cos\Delta_1\cdot\cos\Delta_2\end{bmatrix}$$
$$= f(\Delta_1, \Delta_2) = \boldsymbol{A}\cdot P(\Delta_1, \Delta_2) \quad (4)$$

where Δ_1 and Δ_2 are the phase retardances of two phase retarders, the row vector $\boldsymbol{A} = [a_1, \ldots, a_9]$ consists of the 9 coefficients, and the column vector $[\sin\Delta_1, \cos\Delta_1, \sin\Delta_2, \cos\Delta_2, \sin\Delta_1\cdot\sin\Delta_2, \sin\Delta_1\cdot\cos\Delta_2, \cos\Delta_1\cdot\sin\Delta_2, \cos\Delta_1\cdot\cos\Delta_2]^T$ is denoted as $P(\Delta_1, \Delta_2)$. Equation (4), i.e. $\gamma = f(\Delta_1, \Delta_2)$, is the digital twin that we establish, showing the fact that the optical output power in the system can be expressed as a linear assembly of 9 terms. Once the coefficient vector $\boldsymbol{A}$ is solved, the easy corresponding relation between the optical output power and the phase retardances of two phase retarders can be given by $\gamma = \boldsymbol{A}\cdot P(\Delta_1, \Delta_2)$. Note that a different birefringence of the system corresponds with a different coefficient vector $\boldsymbol{A}$.

The workflow of the digital-twin-based algorithm for real-time polarization tracking is shown in Figure 1b, which can be divided into two steps. The first step is to establish the white-box digital twin by sampling from the real experimental system. First, N ($N \geq 9$) sets of phase retardances $\{\boldsymbol{\Delta}_{(1)}, \ldots, \boldsymbol{\Delta}_{(N)}\}$ are generated, where $\boldsymbol{\Delta}_{(i)} = (\Delta_{1(i)}, \Delta_{2(i)})$ for $i = 1, \ldots, N$, corresponding to two channels of the EPC. The system applies $\boldsymbol{\Delta}_{(i)}$ to the EPC, then samples the output optical power $\gamma_{(i)}$, and repeats this process for N times in total. According to Equation (4), the row vector of output optical power $\boldsymbol{Y} = [\gamma_{(1)}, \ldots, \gamma_{(N)}]$ can be expressed as

$$Y = [\boldsymbol{A}\cdot P(\Delta_{1(1)}, \Delta_{2(1)}), \ldots, \boldsymbol{A}\cdot P(\Delta_{1(N)}, \Delta_{2(N)})] = \boldsymbol{A}\cdot X \quad (5)$$

where X is a 9-by-N matrix depending on the generated phase retardances. Hence, Equation (4) is an overdetermined equation to A. Through solving Equation (5) using the least-squares method, we can obtain the solution $\boldsymbol{A}$, and reconstruct the function $\gamma = f(\Delta_1, \Delta_2) = \boldsymbol{A}\cdot P(\Delta_1, \Delta_2)$. As a result, the white-box digital twin of the entire polarization tracking system is established. The second step is to find the maximum output optical power in the digital twin. The univariate search algorithm is applied to optimize (Δ_1, Δ_2) to maximize the output power $\gamma = f(\Delta_1, \Delta_2)$ and identify the optimal set of phase retardances corresponding to the maximum output power as $\widehat{\boldsymbol{\Delta}} = (\widehat{\Delta}_1, \widehat{\Delta}_2)$. The key point here is that the entire optimization process is carried out in the digital twin, therefore, there are no physical delays induced by various components or systematic instabilities and the optimization process is fast. Finally, the system applies the maximum point $\widehat{\boldsymbol{\Delta}} = (\widehat{\Delta}_1, \widehat{\Delta}_2)$ to the EPC so that the optical output power reaches the maximum value, i.e., the SOP is aligned with the polarizer, thereby achieving real-time polarization tracking. As a reminder, the white-box digital twin does not characterize the input SOP and it merely describes the relation between the output power of the polarizer and the phase retardances of the prior EPC. As a result, like the SPGD, the digital-twin-based polarization tracking can only align the input SOP to the orientation of the polarizer, not an arbitrary SOP.

3. Results and Discussion

The two phase retarders of the EPC used for polarization tracking are scanned to obtain the real mapping between the output optical power after the polarizer and the two phase retardances, as shown in **Figure** 2a. The white-box digital twin established with only 9 samples from the real mapping is shown in Figure 2b. The blue points in Figure 2a indicate the selected 9 samples to create the digital twin. The modeling residuals are directly obtained by subtracting the digital twin from the real mapping, as shown in Figure 2c. Figure 2d displays the histogram of the residuals and the absolute magnitudes of 90% residuals are smaller than 2%. Moreover, the absolute magnitudes of all residuals are less than 5% for all possible phase retardances and the RMSE is 0.012, thereby manifesting the high accuracy of the white-box digital twin.

Different types of polarization disturbances can be achieved by applying different types of driving voltages to the EPC of the polarization scrambler. We use the angle between the Stokes vector after disturbance and the Stokes vector of the original SOP before disturbance to evaluate the magnitude of an SOP disturbance. **Figure** 3a–c displays the recovery curves of the output power, normalized by the average power when no disturbance is imposed, for both the digital-twin-based algorithm and the SPGD when the system encounters different polarization disturbances. The extraordinary peaks close to the maximum are overshoots obtained by the oscilloscope.

We define the time consumed from the polarization disturbance to the average output power of a small continuous time slot (e.g., 0.5 ms here) reaching 98% of the maximum as the recovery time of the algorithm. The recovery time of SPGD varies considerably in different disturbances due to its inherent sensitivity to the initial state. Fortunately, owing to a one-step optimal control strategy governed by strong interpretability, the time-consuming performance of the digital-twin-based algorithm is independent of the initial state, as shown in Figure 3a–c. In principle, the efficiency of the digital-twin-based algorithm is independent from power values obtained during the 9 times of sampling. Mean values and variances of time consumption in 16 different recoveries of the SPGD and the digital-twin-based algorithm are compared in Figure 3d. The digital-twin-based algorithm can ensure the recovery time is within 0.8 ms in any case, and its average recovery time is over 7 times shorter than that for the SPGD. Moreover, the recovery-time standard deviation (STD) of the SPGD is over

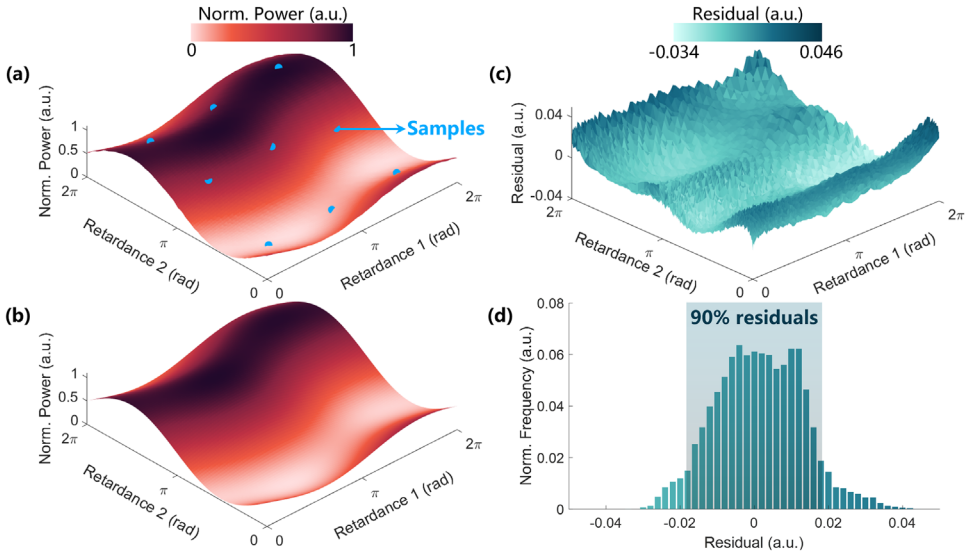

Figure 2. a) The real mapping between the normalized output power and the two phase retardances. b) The established digital twin of the real mapping in Figure 2a. c) The modeling residuals and d) the histogram of the residuals.

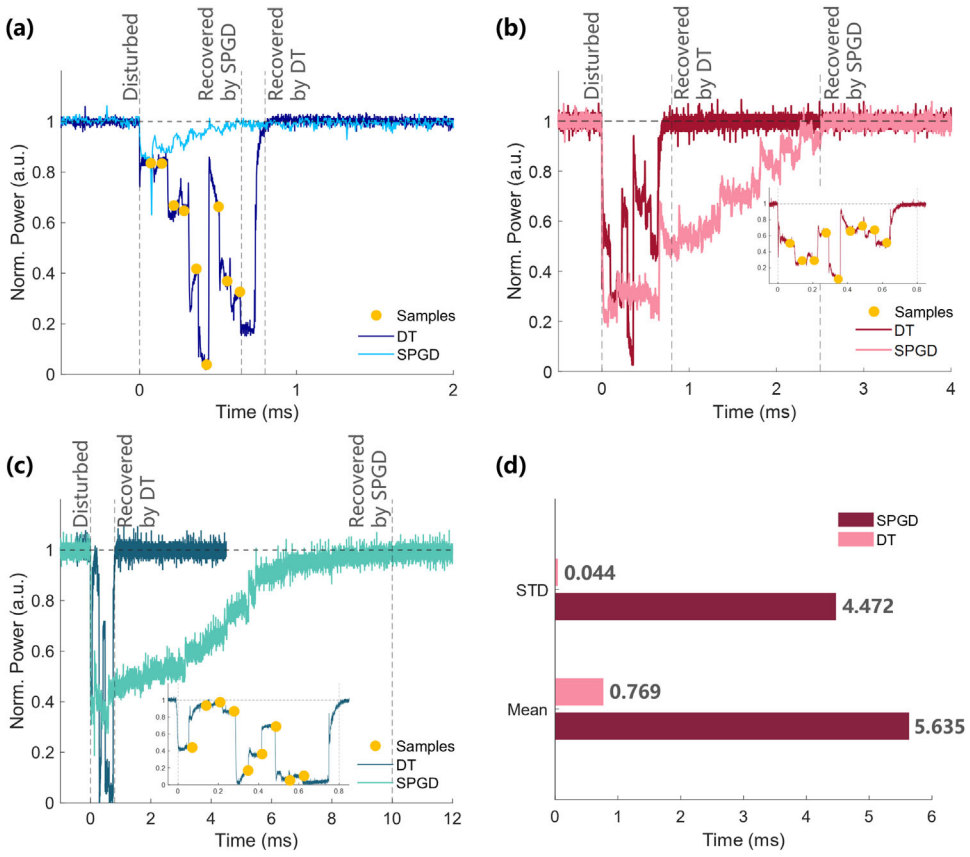

Figure 3. a–c) The recovery curves of both the digital-twin-based algorithm (traces with dark colors) and the SPGD (traces with shallow colors) when the system encounters different polarization disturbances. Nine samples required to establish the digital twin are highlighted in yellow dots. d) Mean values and standard deviations (STD) of recovery time by analyzing 16 different recovery processes.

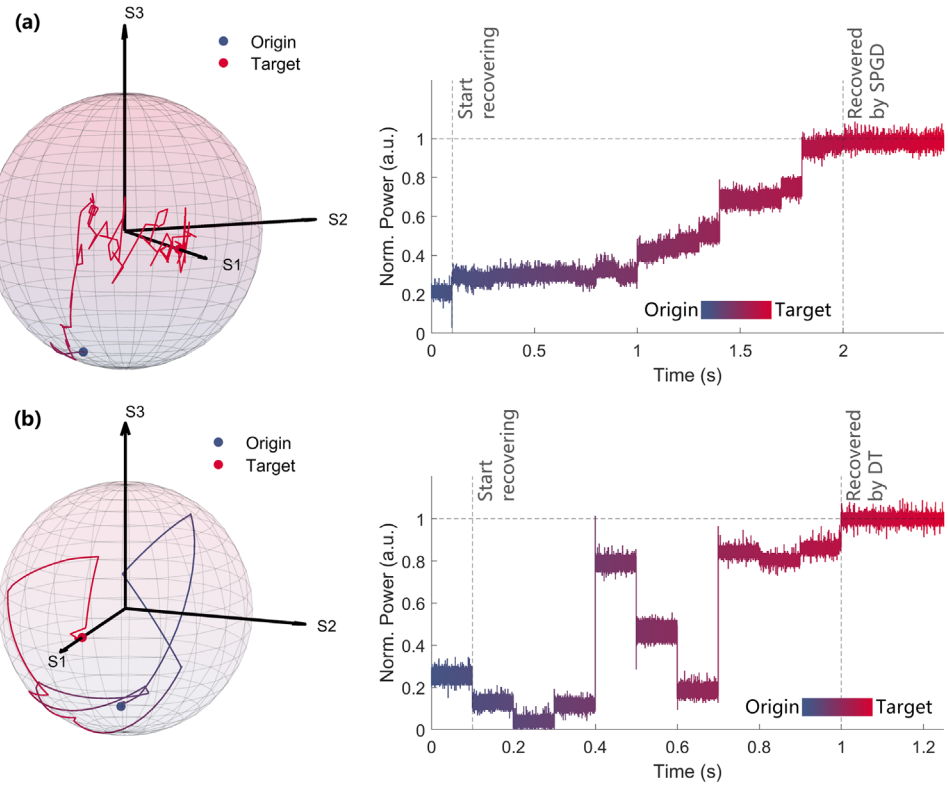

Figure 4. The SOP traces on the Poincaré sphere during the polarization tracking recorded by the polarimeter when the system encounters an identical polarization disturbance and is recovered by a) the digital-twin-based algorithm and b) the SPGD.

100 times larger than that of the digital-twin-based algorithm, validating that the digital-twin-based algorithm is more robust in diverse polarization disturbances. Note that the hyper-parameters of the SPGD are carefully optimized to ensure decent performance.

Figure 4 shows the SOP traces on the Poincaré sphere during the polarization tracking recorded by the polarimeter when the system encounters an identical polarization disturbance and is recovered by the digital-twin-based algorithm and SPGD, respectively. In order to obtain distinct traces and curves under the limited sampling rate of the polarimeter, the delay after every time changing the driving voltages is lengthened to 100 ms. As a result, the time scales of the horizontal axes in Figure 4 become second. The SOP trace of SPGD is twisted while that of the digital-twin-based algorithm is rather straight.

We also characterize the time consumed in waiting for the EPC to respond and in running the algorithm program during the polarization tracking. As shown in Figure 1b, step 1 includes 9 times of sampling and one-step modeling. Every sampling is performed after waiting 50 us to guarantee to obtain stable samplings, which is substantially confined by the response time of the EPC. Each sampling process costs ≈68 us in total. The modeling takes ≈12 us. So, step 1 costs ≈620 us in total. Step 2 includes iterative optimization and typically costs ≈80 us. Step 3 costs ≈68 us to apply the searched phase retardances to the real system. Obviously, ≈65% of the time is consumed waiting for the EPC to respond. Therefore, the time-consuming performance can be further substantially boosted by replacing the current EPC with a faster one.

On the other hand, the major limit in algorithm running would be the iterative optimization, which applies a univariate search algorithm via the digital twin and the optimum is typically located within 10 iterations. During applying the univariate search algorithm, when one variable is fixed, the optimization function turns into a sinusoidal function of the alternative variable. Calculating the optimum of a sinusoidal function consists of multiply accumulation, division, arc-cosine calculation, square and root calculation, and FPGA is rather good at these operations. The FPGA (Xilinx ZC702) has two internal ARM cores and current calculations are actually run in one ARM core based on C language. If the algorithm is realized in Verilog and deployed on the programmable logic gates inside the FPGA, the tracking speed will be substantially enhanced.

Three degrees of freedom are required to transform an arbitrary input SOP to the desired output SOP, which means that using only two phase retarders cannot ensure a complete recovery. In our experiments, the digital-twin-based algorithm with two phase retarders can realize the SOP tracking for most cases, and if not, the digital-twin-based algorithm can guarantee the output power reaching a quite large level, which is at least 90% of the maximum according to our experimental experiences. In this case, the SPGD can be a perfect complement to the digital-twin-based algorithm. We propose a joint algorithm by setting a proper threshold on the output power. When the output power falls below the threshold, it is considered that the system encounters a rather large disturbance hence launching the digital-twin-based algorithm is more efficient. When the output power is still above

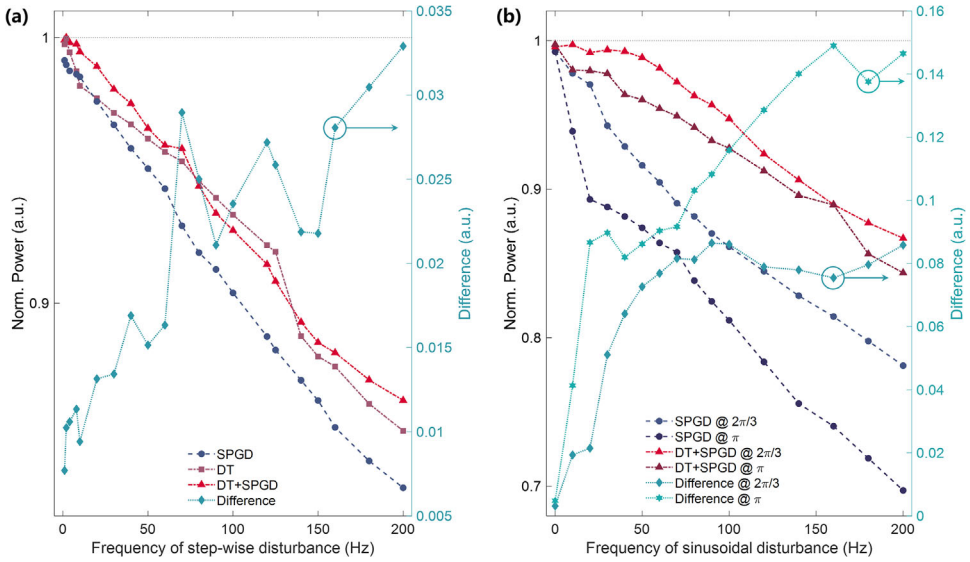

Figure 5. a) The continuous polarization tracking results under step-wise polarization disturbances of the SPGD, the digital-twin-based algorithm (DT), and the joint algorithm (DT+SPGD). The difference between the joint algorithm and the SPGD is plotted on the right axis. b) The continuous polarization tracking results under sinusoidal polarization disturbances of the SPGD and the joint algorithm (DT+SPGD). The differences between the joint algorithm and the SPGD are plotted on the right axis.

the threshold, the SPGD is kept running to deal with small variations. The threshold in the experiments is set as 80% of the maximum output power according to the empiricism. The joint algorithm via combining the digital-twin-based algorithm and the SPGD can avoid the inherent sensitivity to the initial state of the latter, where the SPGD starts with a rather good initial state close to the global optimum quickly obtained by running the digital-twin-based algorithm first. On the other hand, the accidental incomplete recovery when using the two-channel white-box digital twin can be addressed by using a three-channel version of white-box digital twin, i.e. $y = f(\Delta_1, \Delta_2, \Delta_3) = \boldsymbol{A} \cdot P(\Delta_1, \Delta_2, \Delta_3)$, where the vector $\boldsymbol{A}$ consists of 27 elements. As a result, it requires at least 27 samples, which is 3 times that of the two-channel version. Considering the tedious response time of the EPC, the three-channel digital-twin-based algorithm would probably be rather slow. Therefore, we suppose the joint algorithm combining the two-channel digital-twin-based algorithm and the SPGD is the best solution for real-time complete polarization tracking in practice.

To further evaluate the proposed method, experiments of continuous polarization tracking are designed and performed, where the scrambler continuously induces polarization disturbances with certain frequencies. The step-wise and sinusoidal disturbances are realized by applying step and sinusoidal controlling voltages to the EPC of the scrambler. Under continuous disturbances with different frequencies, the output power is measured when using different algorithms for polarization tracking, including the SPGD, the digital-twin-based algorithm, and the joint algorithm. **Figure** 5a shows the experimental results of continuous polarization tracking under step-wise polarization disturbances. The peak-to-peak voltage of the step signal corresponds to the large SOP disturbance of π rad. The output power decreases as the disturbing frequency increases as expected. Both the digital-twin-based algorithm and the joint algorithm outperform the SPGD. The joint algorithm performs best at the majority of disturbing frequencies. As shown on the right axis of Figure 5a, the difference in the output power between the joint algorithm and the SPGD generally increases as the disturbing frequency increases.

We test two types of sinusoidal polarization disturbances, whose peak-to-peak variations correspond to the large SOP disturbance of π rad and the smaller SOP disturbance of $2\pi/3$ rad, respectively. The experimental results of continuous polarization tracking under sinusoidal polarization disturbances are shown in Figure 5b, which further validate the superiority of the joint algorithm. The differences in the output power between the joint algorithm and the SPGD, as shown on the right axis of Figure 5b, again are magnified as the disturbing frequency increases. Particularly, when the frequency of the sinusoidal polarization disturbance reaches 200 Hz, the output power for the joint algorithm is 20% larger than that for the SPGD. Given a certain sinusoidal disturbing frequency, the difference becomes larger when encountering a larger disturbance, suggesting that the performance gap between the joint algorithm and the SPGD increases as the amplitude of disturbance increases. In general, the joint algorithm is more resilient to high-frequency and large-variation disturbances.

We also use the polarimeter to record the SOP with polarization tracking from off to on for both the SPGD and the joint algorithm. **Figure** 6a shows the SOP records under step-wise polarization disturbances, whose intervals randomly range from 20 to 50 ms and peak-peak variations also randomly range from $\pi/3$ rad to π rad. The Stokes vector ($S1$, $S2$, $S3$) of the target SOP is (1,0,0). Figure 6b shows that the variances of the normalized Stokes components of the SPGD are significantly larger than those of the joint algorithm. In particular, the variance of $S1$ for the SPGD is over 20 times larger than that for the joint algorithm, suggesting that the joint algorithm can obtain a much more

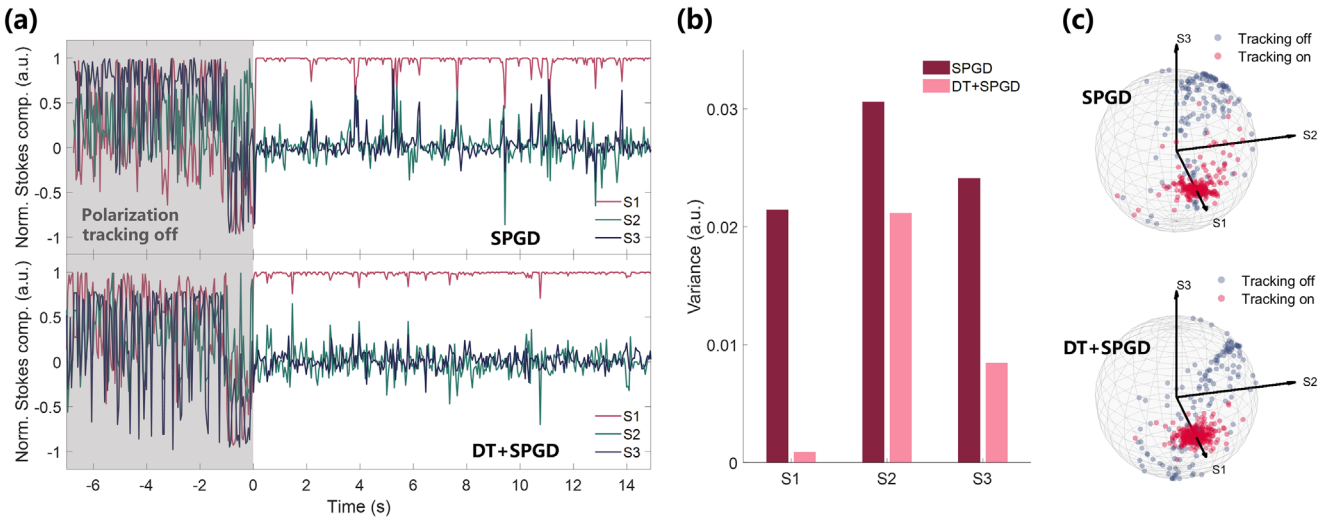

Figure 6. a) Variations of normalized Stokes components when switching polarization tracking from off to on for the SPGD and the joint algorithm (DT+SPGD). b) Variances of the normalized Stokes components with polarization tracking on for the SPGD and the joint algorithm. c) SOP records of the SPGD (top) and the joint algorithm (bottom).

stable SOP than the SPGD can, which is evident in the SOP records shown in Figure 6c. More relevant experimental data supporting the inference can be found in Supporting Information.

4. Conclusion

In conclusion, we demonstrate real-time polarization tracking enabled by a white-box digital twin. Benefiting from the rigorous mathematical derivation with polarization optics, the white-box digital twin can accurately model the entire polarization tracking system with strong interpretability. The adoption of digital twin allows us to bypass the loop of perturbation, sampling, and adjusting over the real system, thereby significantly reducing the sample times and recovery time. Generally, merely 9 times of sampling from the real system is required to establish the digital twin and complete one-step polarization tracking. As a result, the digital-twin-based polarization tracking algorithm averages over 7 times faster than the SPGD. Due to the insensitivity of the initial state, the digital-twin-based algorithm is much more robust than the SPGD in various polarization disturbances. Moreover, by combining the digital twin with the SPGD, more powerful and robust real-time polarization can be delivered in continuous polarization tracking. The novel white-box digital-twin enabled real-time polarization tracking and its variants have great potential in numerous non-polarization maintaining optical systems, whose general performances are related to the stability of SOP.

Supporting Information

Supporting Information is available from the Wiley Online Library or from the author.

Acknowledgements

This research was funded by National Natural Science Foundation of China (grant nos. 62227821, 62025503, and 62205199).

Conflict of Interest

The authors declare no conflict of interest.

Author Contributions

X.Z. and G.P. contributed equally to this work. L.Y. conceived the idea and initiated the research. X.Z. designed the algorithm, performed the experiments, and drafted the manuscript. G.P. contributed to experimental design, data visualization, and manuscript editing. Y.W. assisted in the algorithmic implementation. L.Y., W.H., and G.P. supervised the research. All authors reviewed and approved the manuscript.

Data Availability Statement

The data that support the findings of this study are available from the corresponding author upon reasonable request.

Keywords

digital twin, mueller matrices, real-time polarization tracking

Received: January 16, 2024
Revised: March 14, 2024
Published online: April 16, 2024

[1] S. Wehner, D. Elkouss, R. Hanson, *Science* **2018**, *362*, aam9288.
[2] D. P. Nadlinger, P. Drmota, B. C. Nichol, G. Araneda, D. Main, R. Srinivas, D. M. Lucas, C. J. Ballance, K. Ivanov, E. Y.-Z. Tan, P. Sekatski, R. L. Urbanke, R. Renner, N. Sangouard, J.-D. Bancal, *Nature* **2022**, *607*, 682.
[3] E. D. Caldwell, J.-D. Deschenes, J. Ellis, W. C. Swann, B. K. Stuhl, H. Bergeron, N. R. Newbury, L. C. Sinclair, *Nature* **2023**, *618*, 721.
[4] Y. Lei, F. K. Asadi, T. Zhong, A. Kuzmich, C. Simon, M. Hosseini, *Optica* **2023**, *10*, 1511.

[5] K. Singh, I. Nape, W. T. Buono, A. Dudley, A. Forbes, *Laser Photonics Rev.* **2023**, *17*, 2200844.
[6] H.-S. Zhong, H. Wang, Y.-H. Deng, M.-C. Chen, L.-C. Peng, Y.-H. Luo, J. Qin, D. Wu, X. Ding, Y. Hu, P. Hu, X.-Y. Yang, W.-J. Zhang, H. Li, Y. Li, X. Jiang, L. Gan, G. Yang, L. You, Z. Wang, L. Li, N.-L. Liu, C.-Y. Lu, J.-W. Pan, *Science* **2020**, *370*, 1460.
[7] R. Nozaki, Y. Sato, Y. Shimada, T. Suzuki, K. Yasuno, Y. Ikai, W. Ueda, K. Shimizu, E. Yukawa, K. Sanaka, *Phys. Rev. A* **2023**, *107*, 023707.
[8] I. Walmsley, *Opt. Quantum* **2023**, *1*, 35.
[9] Z. Feng, X. Sun, *Laser Photonics Rev.* **2023**, *17*, 2200961.
[10] M. C. Miller, N. Yunes, *Nature* **2019**, *568*, 469.
[11] K. Nagano, H. Nakatsuka, S. Morisaki, T. Fujita, Y. Michimura, I. Obata, *Phys. Rev. D* **2021**, *104*, 062008.
[12] M. Bailes, B. K. Berger, P. R. Brady, M. Branchesi, K. Danzmann, M. Evans, K. Holley-Bockelmann, B. R. Iyer, T. Kajita, S. Katsanevas, M. Kramer, A. Lazzarini, L. Lehner, G. Losurdo, H. Lück, D. E. McClelland, M. A. McLaughlin, M. Punturo, S. Ransom, S. Raychaudhury, D. H. Reitze, F. Ricci, S. Rowan, Y. Saito, G. H. Sanders, B. S. Sathyaprakash, B. F. Schutz, A. Sesana, H. Shinkai, X. Siemens, et al., *Nat. Rev. Phys.* **2021**, *3*, 344.
[13] Y. Yang, C. Geng, F. Li, X. Li, *Appl. Opt.* **2017**, *56*, 2020.
[14] H. Zhu, X. Duan, S. Fan, H. Wu, X. Lin, Y. Ning, L. Wang, *Opt. Laser Technol.* **2020**, *132*, 106470.
[15] V. Billault, S. Leveque, A. Maho, M. Welch, J. Bourderionnet, E. Lallier, M. Sotom, A. L. Kernec, A. Brignon, *Opt. Lett.* **2023**, *48*, 3649.
[16] B. Y. Kim, Y. Okawachi, J. K. Jang, X. Ji, M. Lipson, A. L. Gaeta, *Laser Photonics Rev.* **2023**, *17*, 2200607.
[17] X. Yang, W. Fu, *Opt. Express* **2023**, *31*, 14403.
[18] T. Lei, C. Zhou, D. Wang, Z. Xie, B. Cai, S. Gao, Y. Xie, L. Du, Z. Li, A. V. Zayats, X. Yuan, *Laser Photonics Rev.* **2022**, *16*, 2100669.
[19] Q. Wu, Y. Zhu, Z. Xu, J. Wei, J. Liang, Y. Yang, G. Qiao, H. Ji, Q. Zhuge, W. Hu, *Opt. Lett.* **2023**, *48*, 4957.
[20] C. De Angelis, A. Galtarossa, G. Gianello, F. Matera, M. Schiano, *J. Lightwave Technol.* **1992**, *10*, 552.
[21] G. D. VanWiggeren, R. Roy, *Appl. Opt.* **1999**, *38*, 3888.
[22] M. Karlsson, J. Brentel, P. A. Andrekson, *J. Lightwave Technol.* **2000**, *18*, 941.
[23] C. Hilweg, D. Shadmany, P. Walther, N. Mavalvala, V. Sudhir, *Optica* **2022**, *9*, 1238.
[24] P. Ju, W. Fan, W. Gao, Z. Li, Q. Gao, X. Jiang, T. Zhang, *Photonics* **2023**, *10*, 6.
[25] K. Singh, I. Nape, W. T. Buono, A. Dudley, A. Forbes, *Laser Photonics Rev.* **2023**, *17*, 2200844.
[26] G. Mamdoohi, A. Fauzi Abas, K. Samsudin, N. H. Ibrahim, A. Hidayat, M. A. Mahdi, *Eng. Appl. Artif. Intell.* **2012**, *25*, 869.
[27] W. Li, X. Zhang, B. You, K. Y. Zou, in *2008 IEEE International Symposium on Knowledge Acquisition and Modeling Workshop* **2008**, pp. 275–278.
[28] Y. Zheng, X. Zhang, Y. Shen, G. Zhou, B. Yang, *J. Opt. Soc. Am. B* **2005**, *22*, 336.
[29] X. Yu-Peng, S. Rong-Tao, L. Xiao, H. Pu, W. Xiao-Lin, X. Xiao-Jun, *Chin. Phys. Lett.* **2012**, *29*, 124212.
[30] R. Su, Y. Liu, B. Yang, P. Ma, X. Wang, P. Zhou, X. Xu, *J. Opt.* **2017**, *19*, 045802.
[31] S. Ren, H. Chang, P. Ma, Y. Chen, G. Wang, W. Li, W. Liu, T. Yao, P. zhou, *Opt. Laser Technol.* **2023**, *166*, 109634.
[32] Q. Xia, J. L. Tao Zhang, J. Yang, Y. He, W. Huang, D. Li, B. Xu, *Acta Optica Sinica* **2020**, *40*, 1526001.
[33] P. H. Lissberger, *Nature* **1977**, *269*, 270.